POLITECNICO DI TORINO
Repository ISTITUZIONALE

Field surveys in heterogeneous rock masses aimed at hydraulic conductivity assessment

Original
Field surveys in heterogeneous rock masses aimed at hydraulic conductivity assessment / Chicco, J.M., Comina, C., Mandrone, G., Vacha, D., Vagnon, F.. - In: SN APPLIED SCIENCES. - ISSN 2523-3963. - 5:12(2023), pp. 1-20. [10.1007/s42452-023-05578-3]

Availability:
This version is available at: 11583/2984190 since: 2023-11-29T09:01:01Z

Publisher:
Springer Nature

Published
DOI:10.1007/s42452-023-05578-3

Terms of use:

This article is made available under terms and conditions as specified in the corresponding bibliographic description in the repository

Publisher copyright

(Article begins on next page)

25 November 2026



Research

Field surveys in heterogeneous rock masses aimed at hydraulic conductivity assessment

Jessica Maria Chicco[1] · Cesare Comina[2] · Giuseppe Mandrone[1] · Damiano Vacha[1] · Federico Vagnon[3]

Received: 4 September 2023 / Accepted: 6 November 2023
Published online: 28 November 2023
© The Author(s) 2023 OPEN

Abstract
In heterogeneous and fractured rock masses, joints are the most important elements controlling the hydraulic conductivity. Joints parameters are therefore crucial for estimating transport of mass and energy in many technical problems (e.g., slope stability, tunnels, geothermal and oil and gas studies). Hydraulic conductivity conceptual models follow well understood generalizations, but their quantitative estimation is not simple. Both laboratory and field tests have many limitations due to representativeness and scale effects. This study proposes a methodology for a preliminary hydraulic conductivity estimation in fractured and/or heterogeneous rock masses through a combination of in-situ geomechanical and geophysical measurements. Contact and no-contact geomechanical surveys were coupled with electric resistivity topographies in two selected test sites within a Mexican geothermal area in the framework of the Ge-Mex H2020 project. The test sites are representative of two different geological settings: a faulted rock mass with expected high hydraulic conductivity in proximity of the faulted areas and an abandoned marble quarry, with very good mechanical characteristics and negligible degree of fracturing. Moreover, both of them are located in remote areas with limited accessibility, in which rapid, time and cost-effective procedures are welcomed and recommended. The preliminary findings of this study were promising: estimated hydraulic conductivities were compared with independent laboratory measurements performed by other researchers showing a good correspondence and reliability. The proposed methodology demonstrated its reliability in decision making, in the technical support and its economical applicability also in similar difficult logistic situations.

Article Highlights

- A combination of in-situ geomechanical and geophysical measurements was adopted for a preliminary hydraulic conductivity estimation;
- Obtained field data were compared with independent laboratory estimations to assess the reliability of the proposed approach and compare representativeness and scale effects;
- Even given the difficult logistic conditions and the limitations of the available comparisons the proposed methodology demonstrated its reliability in decision making.

Keywords Hydraulic conductivity · Rock mass characterization · Geological strength index · Electric resistivity tomography · Mexico

✉ Giuseppe Mandrone, giuseppe.mandrone@unito.it | [1]Interuniversity Department of Regional and Urban Studies and Planning, University of Turin, Turin, Italy. [2]Department of Earth Science, University of Turin, Turin, Italy. [3]Department of Environment, Land and Infrastructure Engineering, Polytechnic of Turin, Turin, Italy.

1 Introduction

Quantitative hydrogeological assessment, in particular hydraulic conductivity estimation, is a key point in many engineering-geological activities, such as underground excavations, hydrocarbon reservoirs and geothermal projects. Understanding geomechanical and thermo-physical features and their relationships with groundwater flow is particularly important in geothermic, especially when facing non-homogeneous rock masses (flysches, calcschists or faulted hard rock lithologies) since joints setting and related parameters can significantly improve the heat transfer mechanism [1]. Particularly in open geothermal systems, where the water is exploited along permeable fractures at depth [2], regional scale groundwater models need to predict: (i) groundwater paths, (ii) properties of the rock medium and (iii) potential water propagation via discontinuities.

Guidelines to define groundwater models at regional scale were developed by many authors, suggesting appropriate methodologies and procedures for fault zone parameterization and representation [3, 4]. A general model conceptualization [5] considers the total width of a fault zone made up of two components: the fault core (FC) and the damage zone (DZ). The FC represents the location of the greatest strain and displacement; the DZ surrounds the fault core, and a smaller amount of strain is here attended. Rawling et al. [6] extended the conceptualization of faults to include a core of low hydraulic conductivity flanked by mixed zones. The main outcome is that faults can broadly exhibit three behaviours in a fluid flow context (Fig. 1a): a barrier to both along- and across-fault flow, (Fig. 1b) a conduit to both along- and across-fault flow and c) a conduit to both along-fault flow and a barrier to across-fault flow.

The hydraulic conductivity estimation in FC and DZ is however complex due to the heterogeneity and anisotropy of rock masses [7]. Many equipment and methodologies have been developed for direct in situ [8] (and reference herein) or laboratory [9] (and references herein) determination. Laboratory measurements are commonly performed on intact or ad-hoc fractured (i.e., with saw-cutting discontinuities) rock samples. Results of these measurements are strongly affected by scale effects (i.e., the centimetric scale of laboratory samples compared to the metric-decametric scale of field fractures), which can lead to considerable misestimations (even some orders of magnitude) with respect to the real in-situ conditions. Indeed, laboratory tests yield hydraulic conductivity values that can be linked to the rock matrix or deep subsurface conditions. In the shallow Earth's crust, conduits, faults, or open discontinuities, in general, facilitate preferential fluid circulation in rock outcrops, and these characteristics are challenging to replicate on a laboratory scale. Moreover, the reduced sample dimensions are not always representative of the whole volume of investigation. Even if direct in situ tests are the most reliable for hydraulic characterization of rock masses, they require big economic and logistic efforts, especially for a preliminary characterization stage, and can be challenging in complex sites conditions.

Consequently, preliminary, and rapid hydrogeological analyses are required and might be performed by using

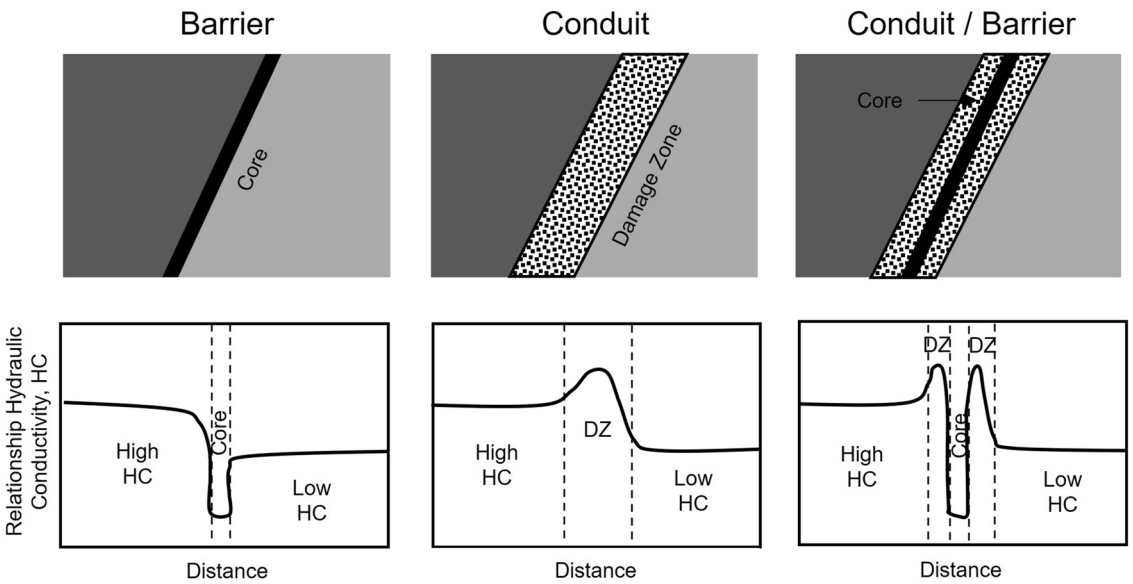


Fig. 1 Three conceptual models of how fault zones impact fluid flow properties (modified after [6])

empirical correlations. The latter can be divided into two main groups: (a) those that evaluate hydraulic conductivity as a function of depth [10–15], and b) those that evaluate hydraulic conductivity as a function of discontinuity features [16] and rock geomechanical classifications [17]. Since stress increases with depth while discontinuity frequency and aperture decrease [18], hydraulic conductivity follows a hyperbolic function with depth. Recent studies focus also on the 3D modelling of fracture paths, however, the higher is the problem complexity, the higher is understanding the sensitiveness of involved parameters [19]. Simplified models were developed for the calculation of hydraulic conductivity by considering discontinuities orientation. For instance, for a planar and parallel discontinuity set [20], conductivity can be estimated by using Richard's equation. For conduits dispersed in orientation, frequency measurements (e.g. volumetric joint count, Jv) and joint orientation allow the evaluation of the contribution of each joint on the conductivity tensor. These approaches are suited for outcrops and surficial flows: it is difficult to use them to reconstruct hydraulic conductivity models at depth, such as for geothermal purposes or deep tunnels.

Hydro-geomechanical classifications were developed to identify bedrock groundwater through the fracture network. As an example, the Hydro-Potential (HP) value technique [17] is based on the modification of the rock mass quality designation (Q-system); the Hydraulic Conductivity (HC) classification [16] by including rock quality designation (RQD), depth index (DI), gouge content designation (GCD) and lithology permeability index (LPI).

Geophysical surveys can be also used to investigate the shallow evidence of geological structures and fractures networks in depth. In recent years, near-surface geophysical prospecting has become a standard tool for the study of faults in a variety of geological contexts (e.g., [21, 22]). When determining the thickness and variability of weathered horizons as well as localized deep fracture zones, Electrical Resistivity Tomography (ERT) in particular was shown to be effective [23, 24]. Many research projects have successfully used ERT to model the petrophysical properties of carbonate aquifers (e.g. [25]), and hard rock aquifers [26]. Other studies have also provided additional quantitative information on the aquifer properties, such as storage properties and recharge processes [27, 28]. However, due to their complexity and lack of data on petrophysical model input parameters, only a small number of studies have evaluated the relationship between geophysical measures and hydraulic properties in hard rock aquifers [29, 30].

To improve the reliability of forecasting hydraulic properties in rock masses, it is essential to couple geophysical surveys with geomechanical investigations, as estimating hydraulic conductivity solely based on geophysical properties can be challenging. A comprehensive multi-scale characterization enables the determination of (a) primary discontinuity attributes (orientation, aperture, and continuity) within the rock mass, (b) interconnections between discontinuities at the outcrop scale, (c) the prediction of discontinuity behavior at greater depths, and d) potential interference of discontinuities with groundwater flow.

Typically, such information is gathered through conventional geomechanical surveys [31]. Today, these surveys can also be enhanced by integrating no-contact investigation techniques like UAV and photogrammetric surveys or laser scanner acquisitions. Consequently, possible misinterpretations of geophysical results can be limited and overcome by the interpretation of geomechanical analyses. For instance, uncertainties arising from high electrical resistivity values, which could be associated with both highly fractured zones under dry conditions or extremely dense and homogeneous material, can be reduced through the findings of geomechanical analyses. Similarly, any fracture infill with clayey materials or water circulation could be identified by combining these investigation methods.

In this paper, geomechanical and geophysical techniques, applied at the outcrop scale, were therefore used to estimate the hydraulic conductivity of two fractured rock masses in the Los Humeros geothermal area (Trans-Mexican Volcanic Belt—TMVB—Mexico). Traditional and no-contact geomechanical surveys and high-resolution ERT have been used to investigate two specific test sites. The combined use of geomechanical and geophysical information allows a first estimation of the hydraulic behaviour of the outcropping rock masses, useful for modelling hydraulic circulation within faulted areas and, more in general, within heterogeneous rock masses. The preliminary results were validated by using independent laboratory measurements performed on the same rock types collected in the surrounding of the test sites. These measurements showcase the promising potential of the proposed methodology, particularly in outcropping rock mass, though primarily at shallow depths.

2 Geological framework of the study areas

Two sites, Rinconada Fault Zone and Granados Quarry (Fig. 2a) at the border of the state of Puebla and Veracruz, were selected to test the proposed approach. In these sites, geological data and boreholes logs showed that discontinuities are the preferred path for fluids circulations, while sound rock hydraulic conductivity is usually considerably neglectable. This is the condition usually characterizing hard rock sites where the rock matrix has generally a

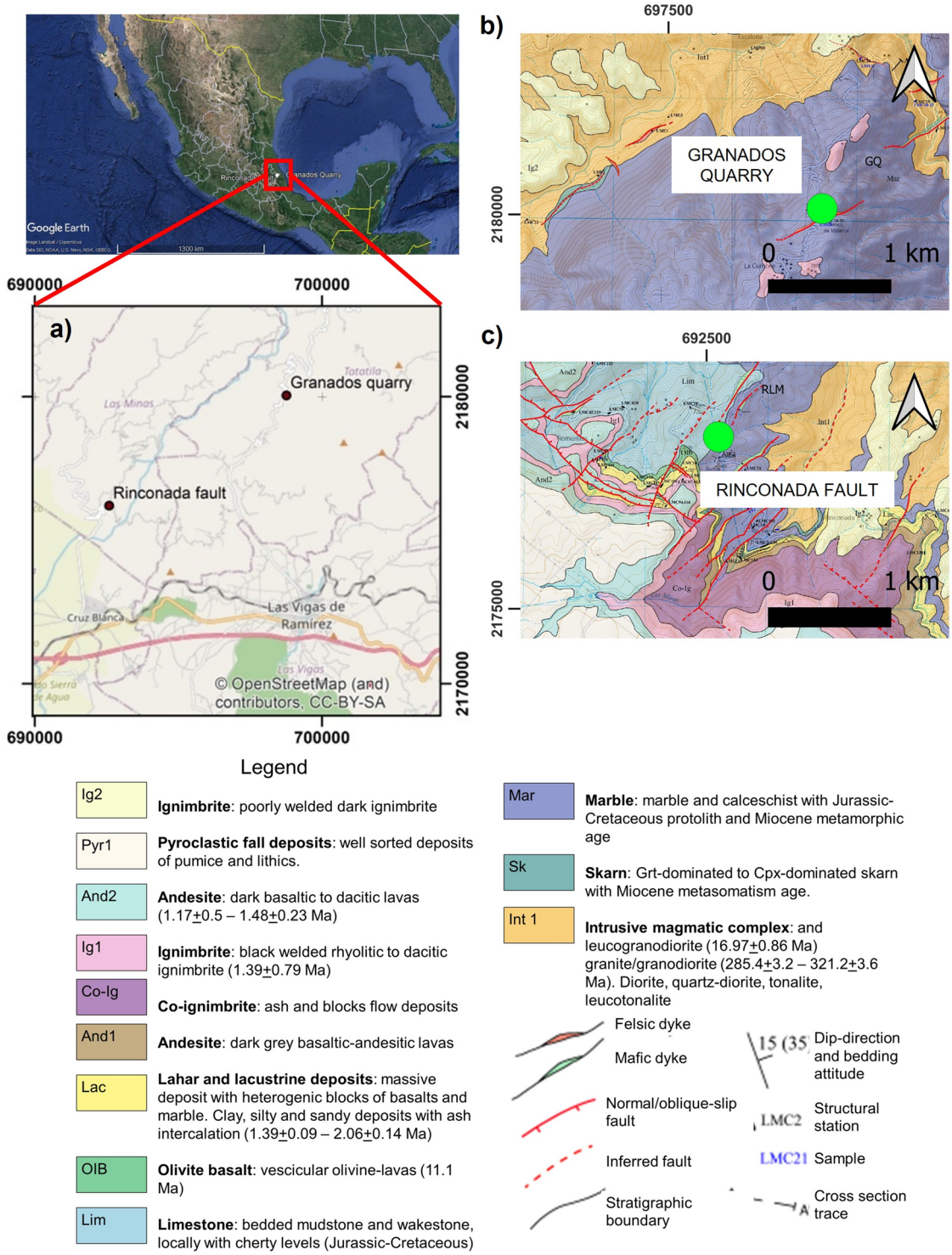


Fig. 2 **a** Location of the study area in GE-Mex H2020 project and location of the two test site in this study (Coordinate system is WGS84/UTM zone 14N). Geological sketch of the fossil hydrothermal system of **b** Rinconada Fault and **c** Granados Quarry (Veracruz, Mexico modified after WP4 GEMex project)

very low hydraulic conductivity compared to the fractured zones.

The Granados Quarry (Fig. 2b) and the Rinconada Fault Zone (Fig. 2c) are located in the Las Minas area, a fossil and exhumed geothermal system considered as an analogue of the active geothermal system of Los Humeros [32]. Strong analogies are mainly referred to the fracture pattern, distribution, and kinematic indicators of fault surfaces of the deep part of Los Humeros reservoir [33], characterized by fractured limestones faulted and intruded by dykes. These fractured host-rocks consists of a low-permeability basement of Cretaceous–Jurassic limestones, partially metamorphosed to marble and skarns by granite intrusions, intensely altered by hydrothermal minerals like calcite, quartz, chlorite, epidote and garnet [34].

From a geological perspective, the past geothermal activity in Las Minas can offer valuable insights into the geological conditions that favoured the development of geothermal systems, potentially resembling those in Los Humeros. This insight is particularly beneficial for comprehending their historical behaviour and potential changes and developments over time. Such knowledge has practical applications for economic purposes, such as implications for energy production, and risk management, including the enhancement of safety measures and the mitigation of potential environmental and geological hazards. Las Minas is located west of the Los Humeros geothermal field, and it crops out in a deeply eroded valley, thus exposing the root of this geothermal system active during late Miocene. The succession of rocks is the same characterizing Los Humeros at depth [35, 36] as highlighted from the borehole logs up to 3000 m: a basement composed of a Paleozoic granodiorite covered by a thick succession of Mesozoic limestones (Cretaceous), intruded by Tertiary (Miocene) dioritic to granitic rocks, and passing upwards to a Quaternary basalt and to dacitic to rhyolitic pyroclastites [37]. Granitic intrusions are responsible for the generation of a thermo-metamorphic aureole made up of marbles and skarns [38]. On top of the carbonatic formations (at about 1500 m depth), a Neogene-Quaternary volcanic succession made of basalts, andesite, ignimbrite and pyroclastic fall deposits can be found. It derives from the evolution of the Los Humeros volcanic complex. Felsic and mafic dykes intrude both the basement rocks and the Pleistocene volcanic units. Plio-Plistocene lacustrine, lahar and pyroclastic deposits filling the tectonic depression can be locally recognized on top of the carbonate rocks and basalts.

Two system of faults, NW- and SW-trending respectively, affect the area crosscutting even Quaternary units. The damage zones of these faults are often mineralized having acted as structural channels during hydrothermalism: they host cogenetic mafic and felsic dykes and rule the skarn distribution [32]. Kinematically, the SW-trending faults are dominantly affected by normal movements while the NW-trending faults are typified by oblique slip movements. The latter system is interpreted as transfer faults, in the frame of the extensional tectonics of the area.

3 Test sites and field surveys

The first test site is an outcrop where the Rinconada Fault is exposed. It is one of the most significant SW-trending faults in the area and it is located to the southwestern most part of the Las minas area (19°40′28.3″ N, 97°09′57.1″ W, Veracruz, Mexico). In the test site, the fault within limestone is very well exposed and shows some marbleization, skarn and a cross-cutting dike (Fig. 3a). The fault core is apparently about 10 m thick. The southern portion is highly fractured for about 20 m. The damage zone is extended also toward the northern side of the fault, and is characterized by a poorly interlocked, heavily broken rock mass with mixture of angular rock pieces in a finer matrix. Only the southern side of the fault is feasible for geomechanical surveys (A–A′) while the opposite one was investigated with a ERT survey (B–B′). Indeed, geomechanical and geophysical surveys have contrasting site requirements for their execution: for the first a clear outcrop of the rock mass is necessary (in this specific site only the southern side of the fault is well exposed) while for the second the availability of some accessible space with nearly linear extension is necessary to deploy the instrumentation (in this specific site only the northern portion of the road provided enough space for the surveys). Both traditional geomechanical surveys and no-contact surveys investigated the area (Fig. 3b). The very core zone of the fault (1–2 m of crushed-like accumulation) is missing due to the complete destruction of the rock mass.

The second test site is in the Granados Quarry (19°42′21.30″ N, 97°6′13.11″ W, Tatatila, Veracruz, Mexico). It is a marble quarry with sub-vertical mafic intrusions and minor faults (Fig. 4). The marble quarry is located in the same hydrothermal system of Rinconada Fault: here, Miocene dioritic intrusions generated a thick contact aureole of HT-metamorphism, thus the rock types belonging to the Cretaceous limestone unit widely metamorphosed to marbles. Marble is white to light grey and locally mottled due to the presence of wollastonite and Fe-Oxide. Karst activity is widespread in the area. In this case study there is a small dyke (20 cm) and two large dykes (2–3 m subvertical, 1.5 m dipping about 60°) cutting the marble. The 1.5 m thick dyke has a syn-intrusion fault-like damage zone. Geomechanical and geophysical surveys were executed on a lateral front of the quarry. The geomechanical scanline (C–C′) was materialized on the uppermost quarry

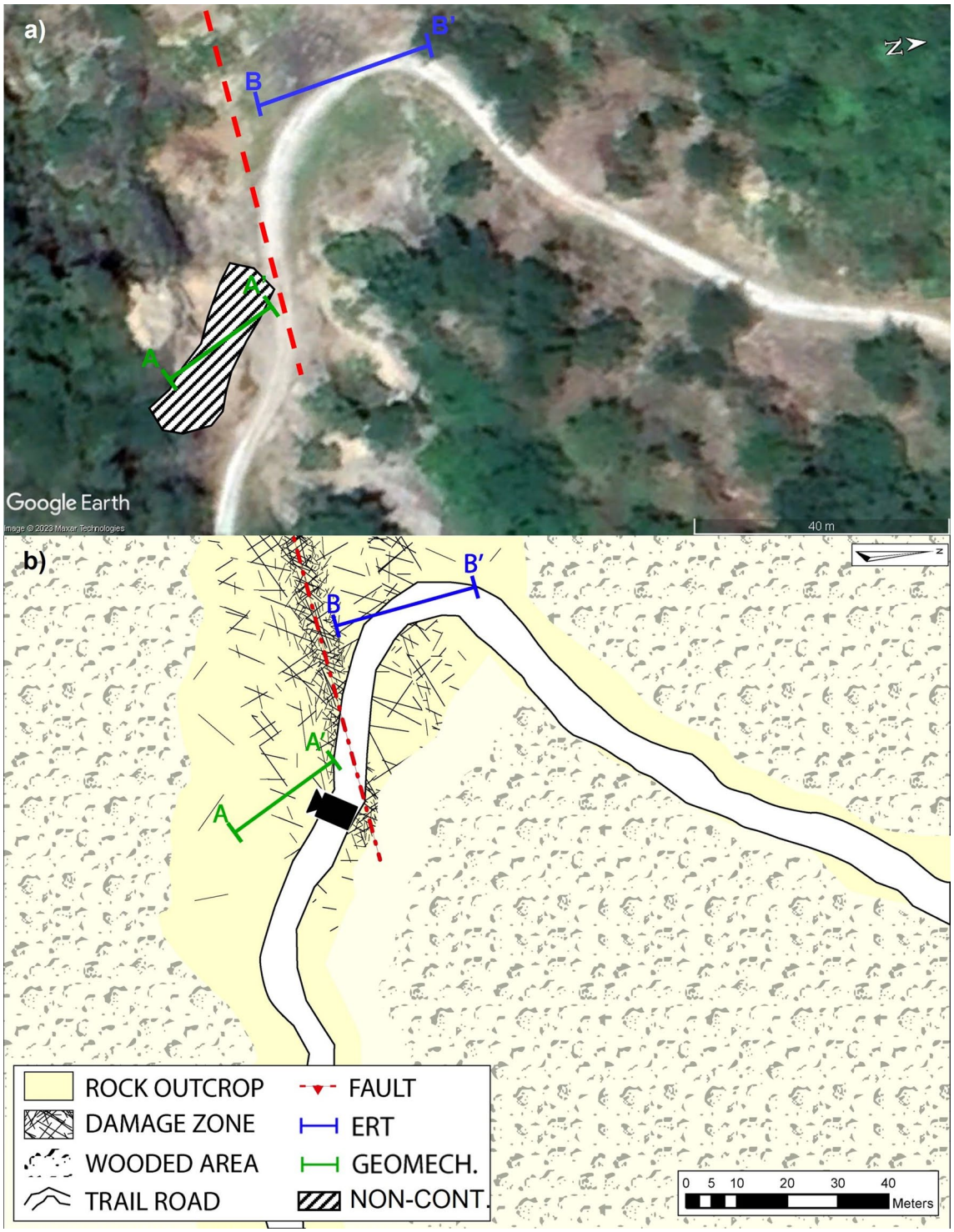


Fig. 3 **a** Aerial view of the Rinconada Fault (red dashed line) site. **b** Planimetric sketch of the Rinconada Fault site and executed surveys. The black camera represents the shooting point of the no-contact survey: the area covered by no-contact survey has an extension corresponding to AA' profile length

front, which was also the subject of no-contact surveys. The ERT profile (D–D') was executed at the base of the front itself, aimed at investigating the relationship of the dike (Fig. 4b, c). Choice of the survey's positions followed considerations similar to the ones reported above: only the uppermost quarry front had a well exposed outcrop

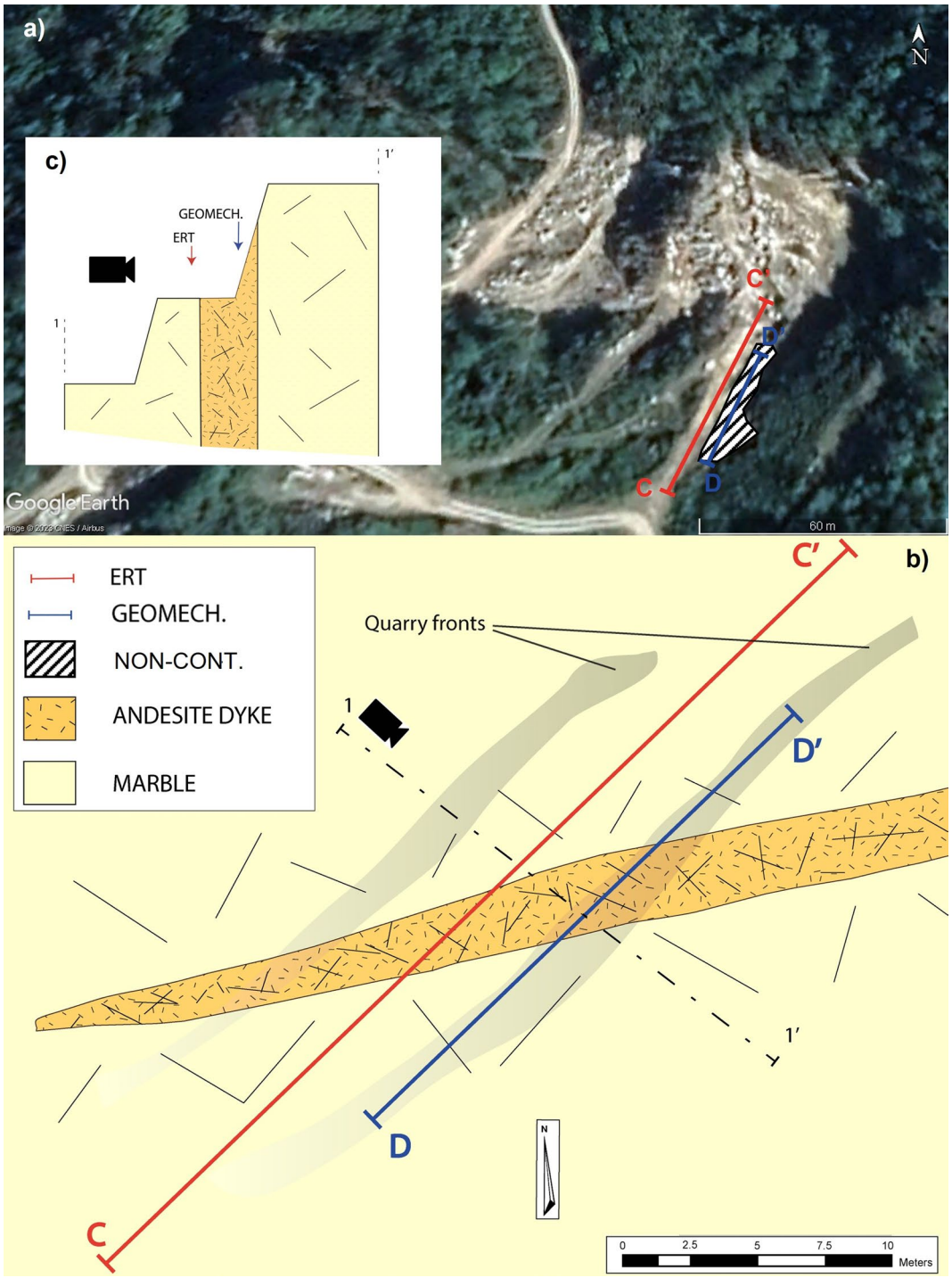


Fig. 4 **a** Aerial view of the Granados quarry site and of the executed surveys: **b** planimetric sketch and **c** cross-section following 1–1′ trace drawn in panel **b**). The black camera represents the shooting point of the no-contact survey: the area covered by no-contact survey has an extension corresponding to DD′ profile length

(the lowermost front was partially covered with debris and alteration material) while only in the lowermost front there was enough space for the geophysical survey alignment.

The combined use of geomechanical and geophysical surveys was used to investigate fractured outcrops and develop a hydrogeologic model for reconstructing the behaviour of faulted areas. As already remarked, surveys were executed in areas of the sites where it was logistically possible to locate the survey lines. Due to this logistical consideration, there is not a perfect correspondence

between the geomechanical and geophysical surveys at the study sites. Nevertheless, we do not view this as a limitation of the work since the primary aim of the surveys was to integrate the two methodologies rather than directly comparing them in the same location. Even though the surveys were not conducted in the same positions, the results from both surveys mutually validate each other since they reveal similar site settings.

The conceptual workflow (Fig. 5) we adopted was aimed at: (a) provide a first order hydraulic conductivity estimation from geomechanical data for the zone where geomechanical surveys (both contact and no-contact) were possible to be executed, (b) extend the information on the site setting from geomechanical characterization in the underground through the use of geophysical surveys providing a link between resistivity properties and geomechanical properties and (c) allow the identification of the main fracture settings controlling water and thermal flows at the sites by merging all the results acquired.

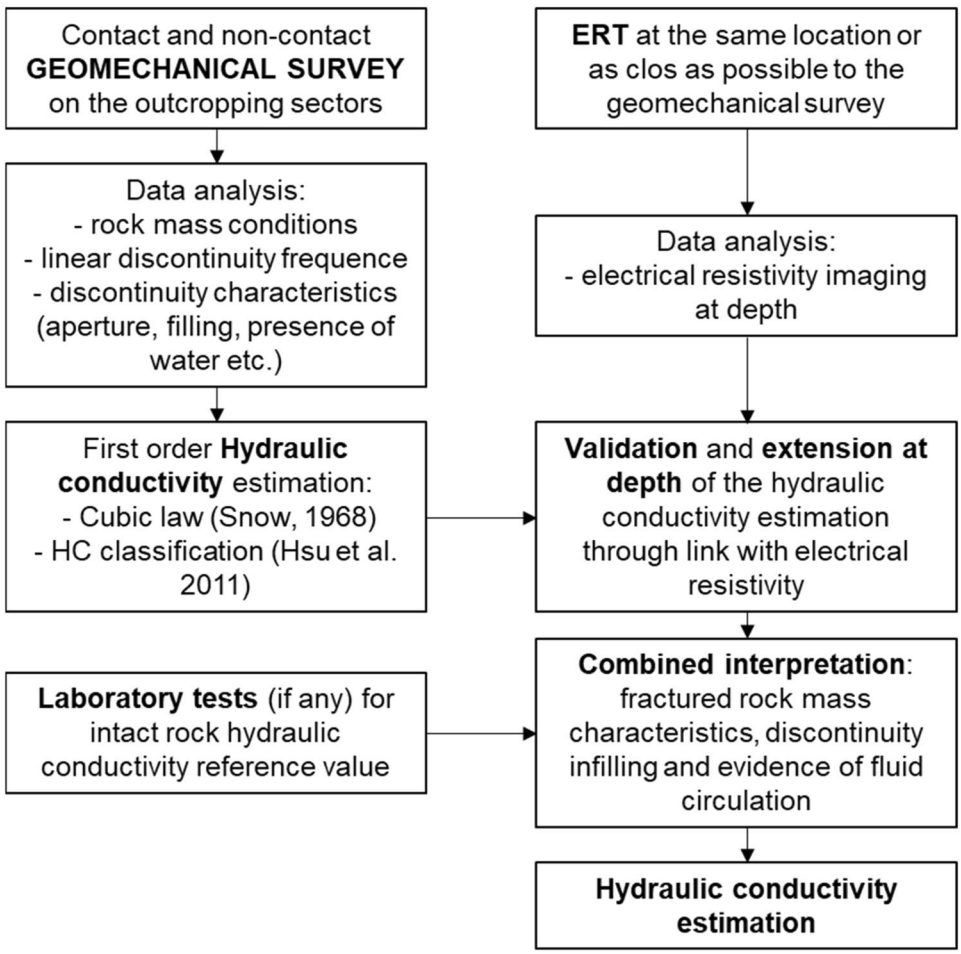


Fig. 5 Conceptual workflow of the proposed procedure for the hydraulic conductivity estimation in heterogeneous rock mass

Table 1 Summary of the geomechanical and geophysical surveys performed in the test sites

Site	Geomechanical surveys			Geophysical survey	
	Traditional	No-contact		Length [m]	Depth of investigation [m]
	Length [m]	Number of photos	Point density[number of points/m^2]		
Rinconada Fault	20	25	2.2×10^4	48	6
Granados Quarry	22	18	1.8×10^4	48	8

4 Materials and methods

In the following sections, a detailed description of the techniques used in the two test sites is provided. In Table 1 are summarized the main characteristics of the performed geomechanical (both traditional and no-contact) and geophysical surveys.

4.1 Geomechanical surveys

Traditional geomechanical surveys were carried out to identify the number of families/systems and to associate a representative value of orientation, spacing and frequency, persistence, roughness, wall strength, opening, filling and hydraulic conditions to each family, according to [31] suggestions, on directly accessible sectors of the two sites (Figs. 3b and 4b).

No-contact measurements investigate inaccessible portions of the outcropped fault zones too (Figs. 3b and 4b). Photogrammetric surveys and numerical elaborations were conducted to produce 3D models of the outcrops. The camera used was a rugged PENTAX WG-3 GPS equipped with a 1/2.3" BSI-CMOS 16 MP sensor and a built-in GPS. Image acquisition was done overlapping images acquired with the hand-held camera. Model orientation was performed using the internal GPS and then refined by aligning the dense point cloud with in-situ surveyed control points. Tie point extraction, bundle block adjustment, dense image matching and 3D photogrammetric modelling have been done using the Photoscan® software. The obtained aligned and scaled clouds were interrogated thought CloudCompare® for measuring structural data using the Compass plugin. The technique involves identification on the RGB image of the best-exposed planes and subsequent geometric measurement of individual points lying on the plane. At the end of the process, a best fitting of the measured points ensures the identification of the plane corresponding to the orientation of the discontinuity. Only when adequate convergence on the orientation of the plane is achieved it is selected and used in the geomechanical interpretation (red polygons in the Figs. 6 and 9).

Field data were used to classify rock masses using Geological Strength Index [39], and result were compared to the no-contact geomechanical data.

4.2 Geophysical surveys

Electrical Resistivity Tomographies (ERT) were executed on both sites to image the resistivity distribution at depth and correlate it to the surface evidence coming from the geomechanical surveys. Particularly the imaged resistivity values of the different portions of the reconstructed sections were attributed to different fracture settings (and consequently different hydraulic conductivity properties) comparing the data obtained at depth with the geomechanical surveys in the same portions of the sections or in portions that can be hypothesized to have a similar geological structure. A Syscal-Pro® acquisition device was adopted with 48 measuring electrodes. Two different acquisition sequences have been used, eventually combined in a single dataset to improve lateral resolution and investigation depth: a Wenner-Schulumberger quadrupole configuration, involving a total of 871 potential measurements along the section, aimed at increasing the penetration depth of the surveys; a Dipole–Dipole quadrupole configuration, involving a total of 497 potential measurements along the section, aimed at increasing the lateral resolution of the surveys.

Experimental data were inverted with Res2DInv® after partial filtering of anomalous measurements (std > 5%). A

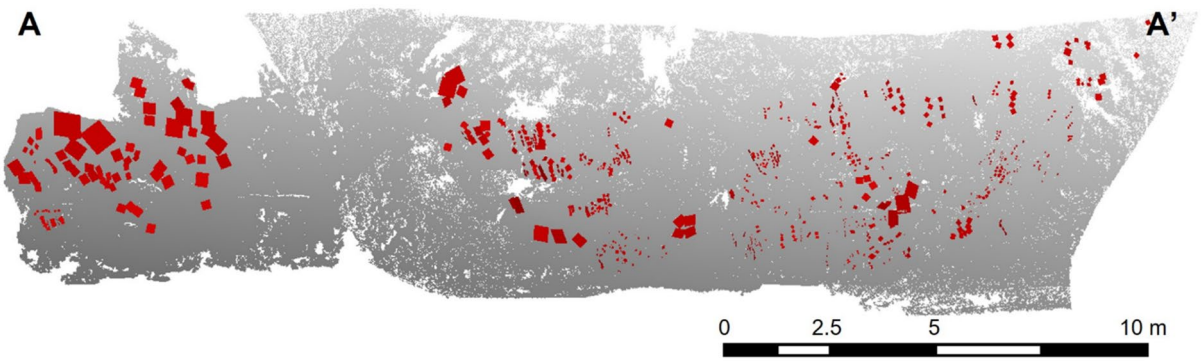


Fig. 6 Plane extraction from the point cloud at Rinconada fault in the same area of the traditional geomechanical survey, in red the polygons with adequate convergence on the resulting plane orientation adopted in the study are evidenced. For location of the survey line see Fig. 3

very good convergence of the results has been obtained from the inverted resistivity models with a global rms below 3%.

5 Results

The two sites represent different example of geological frameworks and results that can be achieved are partially different. In both cases, geomechanical and geophysical surveys allowed to improve substantially the knowledge that can be ascertain from the outcrop analysis and give interesting outputs with respect to the continuation of the imaged fractures at depth and the potential correlation between fracture setting and electrical resistivity that can be helpful also for further studies.

5.1 Rinconada fault

At the Rinconada fault site, 3 principal sets of discontinuities were identified from field measurements: the most representative one is a set oriented 75/345 (K1), almost parallel to the fault. A perpendicular set is 80/270 (K2) while a minor one shows an orientation of about 80/265 (K3). The spacing increase moving away from the fault core, ranging from few centimetres to 1 m or more, same for the persistence. The discontinuities are closed and no—or slightly—weathered. Rock mass characterization was done each 2 m going apart from the core zone of the fault aiming at describing differences from the core zone to the sounding rock mass.

On the 3D point cloud 884 planes were manually drawn (red polygons in Fig. 6) and their orientations were extracted. Three main discontinuity sets were recognized. The mean set planes are respectively 70/355, 80/265 and 75/55 (sub-vertical), in very good agreement with field survey. The median spacing values are the following: 0.02 m for K1, 0.09 m for K2 and 0.11 m for K3.

In Table 2 are shown results from contact survey, in particular Volumetric joint count (Jv), Rock Quality Designation Index (RQD), Rock Mass Rating (RMR) and Geological Strength Index (GSI). In Fig. 7, the variation of the discontinuity frequency or linear intensity [40], is provided too.

The geoelectric survey investigated the northern side of the fault core, acquiring the section along the road, perpendicularly to the fault plane trace on the horizontal plane. The resistivity section (Fig. 8) highlights the presence of a highly resistive anomaly (around 3000 Ohm.m) in the far field towards north (B'). This anomaly can be correlated to the massive sector of the fault zone, made of less fractured rocks (blocky to massive in Fig. 8). The highly fractured zone between this sector and the fault core, which is the starting of the profile (B), has a relevant extension (> 20 m) suggesting significant fault movements (very blocky to crushed in Fig. 8). From a technical point of view, the resistivity distribution shows the same succession depicted by the geomechanic surveys (on the other side of the fault), from the intact rock mass to the fault (blocky-disturbed-very blocky-disturbed).

5.2 Granados quarry

A lateral scarp of the marble quarry was investigated. Most of the joints are oriented 85/160 (in the andesitic dike the orientation seems changing towards 85/340). Joints are very persistent and the spacing ranges from 30 to 80 cm. Joints belonging to the sets oriented 80/050 and 75/195 are less abundant: in this case spacing is slightly less than 1 m and persistence range from decimetres to meters. Joints show generally a slight alteration (more evident in the dike) and in most cases are open (andesite, about 1 mm in mode value within 31 joints) or juxtaposed (marble, about 0.5 mm in mode value within 65 joints). Most of the joints in the andesite are filled with soft clay and traces of humidity, even if the rest of the outcrop was dry.

Table 2 Rock mass characterization each 2 m along the field scanline. The origin of the scan-line is in A' in Fig. 7

Distance from the origin [m]	No. of joints	No. of families	Jv [j/m3]	RQD	RMR	Class	GSI	Description
0–2	18	1	14.4	67.4	61	2	56	Very blocky
2–4	20	2	20.4	47.6	57	2	52	Very blocky
4–6	23	2	23.4	37.7	57	3	52	Very blocky
6–8	10	1	8	88.6	68	2	63	Very blocky
8–10	7	1	5.6	96.5	73	2	68	Blocky
10–12	5	1	4	100	73	2	68	Blocky
12–14	10	1	8	88.6	68	2	63	Very Blocky
14–16	4	1	3.2	100	73	2	68	Blocky
16–18	6	1	4.8	99.1	73	2	68	Blocky
18–20	5	1	4	100	73	2	68	Blocky

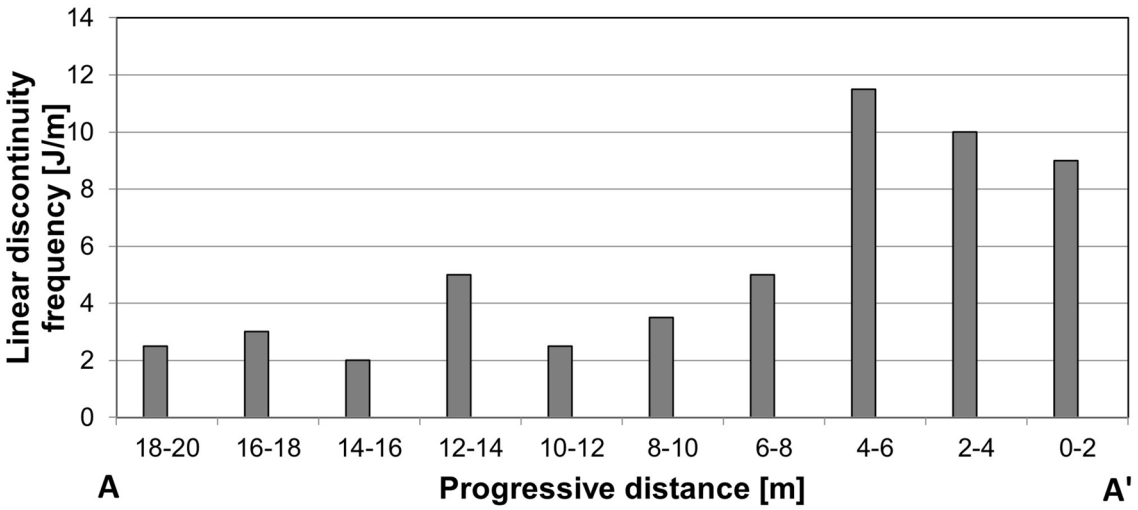


Fig. 7 Discontinuity frequency for the Rinconada Fault site: the fault core is on the right side, beyond the first class (0–2 m). For location of the survey line see Fig. 3

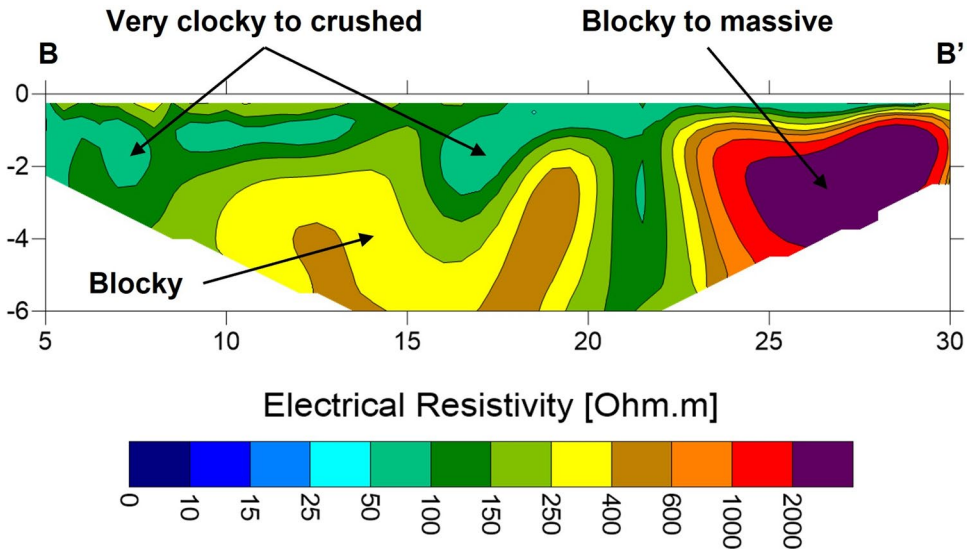


Fig. 8 Imaged resistivity distribution along the Rinconada Fault section. For location of the survey line see Fig. 3

Discontinuities were recognized also by manual measurements on the 3D points cloud (Fig. 9) and dip and dip directions were assessed: 703 planes orientations were used to implement statistical analysis (i.e. mean and median analyses over the different fracture clusters evidenced by the isolated planes) which indicates the presence of 5 main discontinuity sets oriented 75/182 (k1), 84/232 (k2) and 13/160 (k3), 80/27 (k4) and 65/350 (k5) respectively. The real spacing for each of the main sets was also evaluated: median values are 0.07 m for k1, 0.20 m for k2, 0.5 m for k3, 0.04 m for k4 and 0.02 m for k5. Persistence measurements were also conducted on the whole discontinuity database. Data shows a minimum value of 0.05 m, a maximum of 7.93 m, a mean of 0.76 m and a median of 0.49 m: the trend follows a typical (for persistence) log-normal distribution.

The discontinuity frequency analysis, both in situ (Table 3) and by following a virtual scanline materialized on the 3D model, gives global linear frequency values which mimics the lithotecnical units detected in the field (Fig. 10): this value is lower in the marble portions, while in correspondence of the andesite intrusion it increases. This trend is evidenced in the graph, were one-meter stepped and lithotecnical unit averaged value of the fracture density is shown.

In the same location a resistivity section was acquired along a quarry road at the base of the outcrop already described. It was intended to image eventual differences

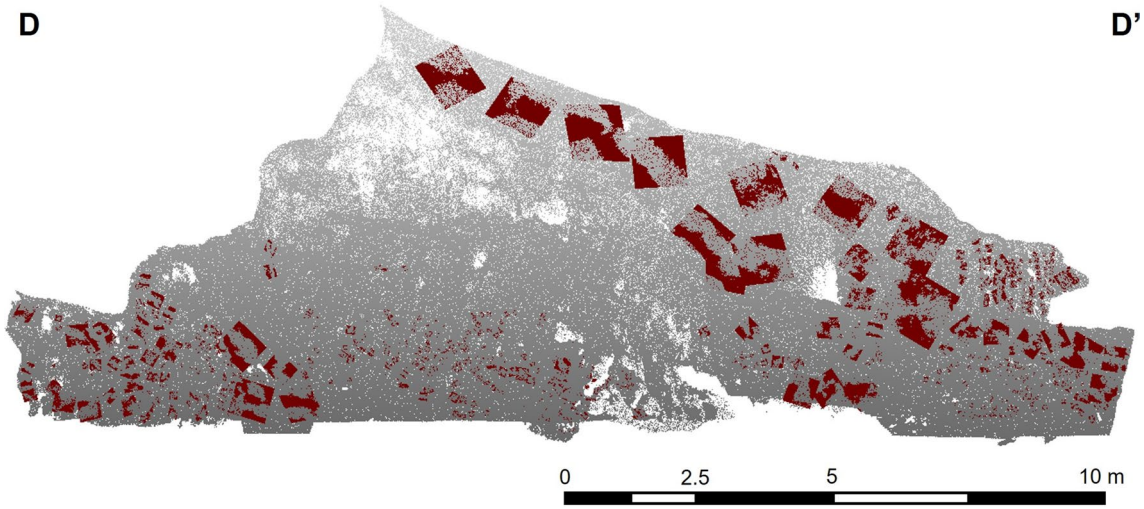


Fig. 9 Plane extraction from point cloud—Granados Quarry, in red the polygons with adequate convergence on the resulting plane orientation adopted in the study are evidenced. For location of the survey line see Fig. 4

Table 3 Homogeneous intervals of observation along the scan line highlighting how the number of joints and the GSI change with the lithology

Distance from the origin [m]	n. of joints	GSI	Lithology	Note
0–2	6	85	Marble	
2–4	6	85	Marble	
4–6	6	75	Andesite	Cataclastic with clay
6–8	9	75	Andesite	clay infilling
8–10	9	70	Andesite	Cataclastic
10–12	4	80	Marble	
12–14	5	85	Marble	
14–16	6	85	Marble	
16–18	4	85	Marble	
18–20	3	85	Marble	
20–22	3	85	Marble	

in resistivity distribution due to the passage along the subvertical mafic intrusion and describe the continuity in the underground.

Particularly the presence of the mafic intrusions and minor faults is interesting with respect to the Los Humeros reservoir and poorly investigated. In fact, due to the high thermal properties of these mafic rocks, potential thermal pathways are expected in these areas. Moreover, the fracturing created as a consequence of the mafic rock intrusion is favourable for fluid circulation, which might increase the overall temperature of the reservoir.

From the reconstructed resistivity section (Fig. 11), it is possible to visualize a highly resistive formation (around 15,000 Ohm m) related to the presence of compact marble formation in the NE part. This formation is truncated by a vertical steep low resistivity (4 Ohm m) anomaly, which matches with good approximation the location of the Mafic dyke evidenced in the outcrop (see Fig. 4). The evidenced anomaly characterizes the whole investigated depth (about 10 m). The low resistivity of this portion suggests a strong elaboration of the related material and the presence of alterations. On the SW side of this inclusion (towards C) the marble formation is again encountered even if showing lower resistivity values (around 4000 Ohm m) with respect to the same marble in the NE (towards C') side. This difference appears to roughly match the evidence from geomechanic surveys, reporting a more fractured domain corresponding to the andesitic dike, and two less fractured domains ascribed to the marble.

6 Hydraulic conductivity estimations

The geomechanical characterization allowed the estimation of hydraulic conductivity in the two-test site in proximity of the fault zone. Among the available methodologies, the Snow's (1968) cubic law and the HC classification [16] were applied to the test sites.

By assuming parallel and planar joints [20], hydraulic conductivity can be evaluated based on the geomechanical surveys using the cubic law as in the following:

$$K = \frac{e^3 \cdot g \cdot f}{12 \cdot \nu} \quad (1)$$

where e is the fracture opening, g is the gravity force, f is the frequency of discontinuity, and v is the water kinematic viscosity. Equation 1 shows that the fracture aperture is

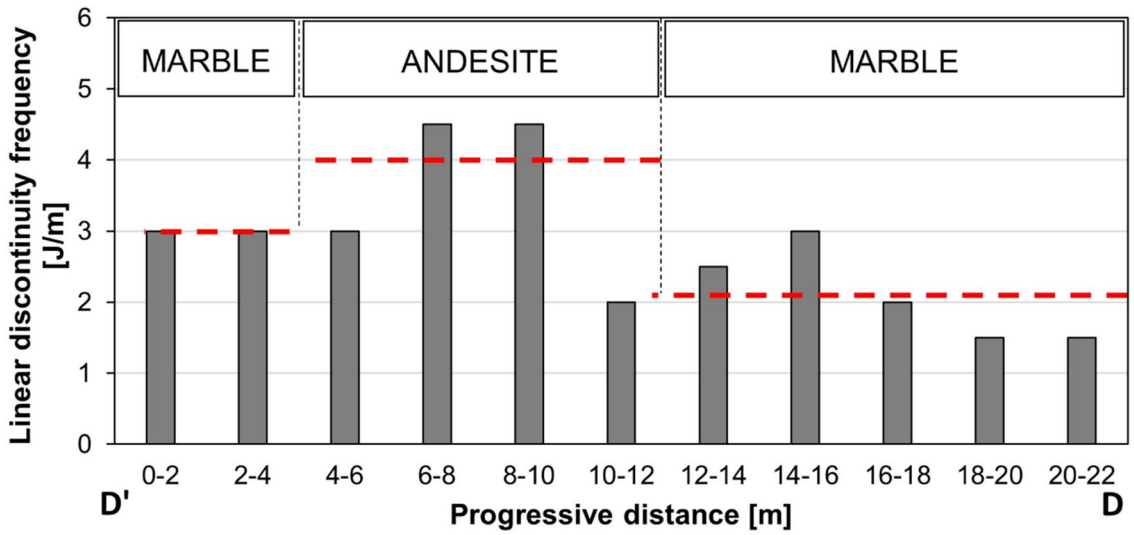


Fig. 10 Linear discontinuity frequency (gray = raw data; red = mean value for the corresponding lithology) derived from points cloud analysis. For location of the survey line see Fig. 4

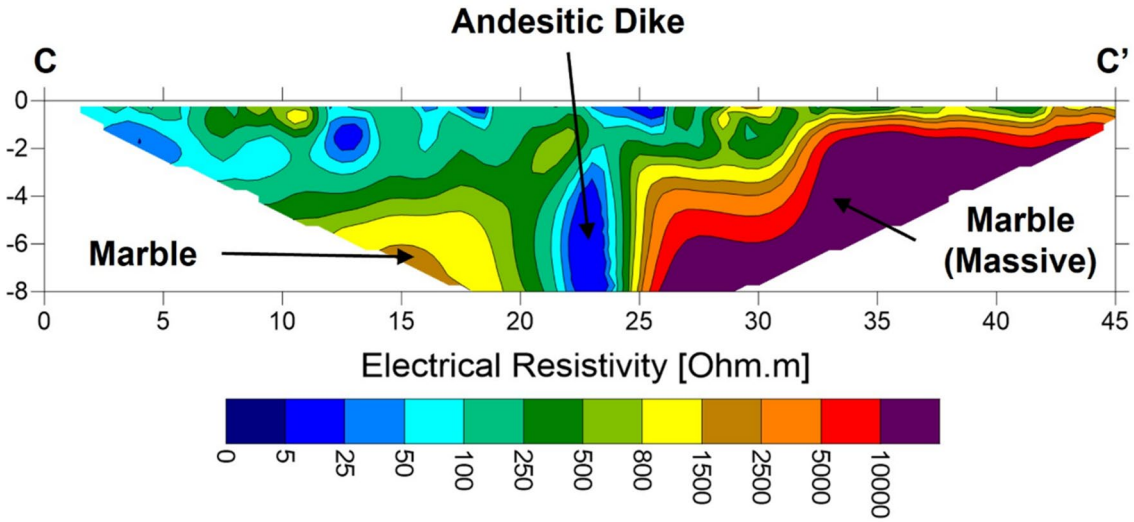


Fig. 11 Imaged resistivity distribution along the Granados quarry section. For location of the survey line see Fig. 4

more important than fracture density for determining the hydraulic conductivity [41].

For each test site, based on geomechanical measurements, opening values were estimated varying between 0.5 mm near the fault and 0.01 mm in the sounding rock sectors. In particular, 150 joints opening values were used for statistical analysis: raw opening data ranged from more than one millimetre in the fault area to negligible opening away from DZ. Moreover, the median discontinuity frequency value for each rock mass type was used for the calculation of hydraulic conductivity.

The HC classification [16] was also applied to the two test sites. The HC classification provide a HC value that range between 0 and 1. HC values are given by:

$$HC = \left(1 - \frac{RQD}{100}\right) \cdot DI \cdot (1 - GCD) \cdot LPI \quad (2)$$

where DI is the depth index, GCD is the gouge content designation and LPI is the Lithology Permeability Index. Hsu et al. [16] also proposed the following equations to relate HC with K:

Table 4 Determination of K values by using cubic law model and HC classification and comparison with lab hydraulic conductivity (after [9]) on similar rock samples

Site	Scan-line sectors [m]	RQD	Cubic law [20]			HC classification [16]					Lab K[m/s]
			e[m]	F [1/m]	K [m/s]	DI [-]	GCD [-]	LPI [-]	HC	K[m/s]	
Rinconada Fault	0–2	67.4	5.00E-04	9	9.20E-04	1	1	0.7	0.228	3.90E-07	2.5E-09 + 9.3E-09
	2–4	47.6	5.00E-04	10	1.02E-03	1	1	0.7	0.367	7.52E-07	
	4–6	37.7	5.00E-04	11.5	1.18E-03	1	1	0.7	0.436	9.54E-07	
	6–8	88.6	1.00E-04	5	4.09E-06	1	1	0.7	0.080	9.16E-08	
	8–10	96.5	1.00E-04	3.5	2.86E-06	1	1	0.7	0.025	1.80E-08	
	10–12	100	1.00E-04	2.5	2.04E-06	1	1	0.7	0.007	3.19E-09	
	12–14	88.6	1.00E-04	5	4.09E-06	1	1	0.7	0.080	9.16E-08	
	14–16	100	1.00E-05	2	1.64E-09	1	1	0.7	0.007	3.19E-09	
	16–18	99.1	1.00E-05	3	2.45E-09	1	1	0.7	0.006	2.76E-09	
	18–20	100	1.00E-05	2.5	2.04E-09	1	1	0.7	0.007	3.19E-09	
Granados Quarry	0–2	96.3	1.00E-05	3	2.45E-09	1	1	0.7	0.026	1.93E-08	1.7E-08 + 4.3E-08
	2–4	96.3	1.00E-05	3	2.45E-09	1	1	0.7	0.026	1.93E-08	
	4–6	96.3	1.00E-05	3	2.45E-09	1	1	0.7	0.026	1.93E-08	
	6–8	92.5	1.00E-05	4.5	3.68E-09	1	1	0.7	0.053	5.18E-08	
	8–10	92.5	1.00E-05	4.5	3.68E-09	1	1	0.7	0.053	5.18E-08	
	10–12	98.2	1.00E-05	2	1.64E-09	1	1	0.7	0.012	6.91E-09	
	12–14	97.4	1.00E-05	2.5	2.04E-09	1	1	0.7	0.019	1.22E-08	
	14–16	96.3	1.00E-05	3	2.45E-09	1	1	0.7	0.026	1.93E-08	
	16–18	98.2	1.00E-05	2	1.64E-09	1	1	0.7	0.012	6.91E-09	
	18–20	99.0	1.00E-05	1.5	1.23E-09	1	1	0.7	0.007	3.27E-09	
	20–22	99.0	1.00E-05	1.5	1.23E-09	1	1	0.7	0.007	3.27E-09	

$$K = 3 \cdot 10^{-6} \cdot (HC)^{1.38} \quad (3)$$

In the test sites, RQD was inferred from geomechanical surveys; DI, GCQ and LPI were respectively considered equal to 1, 1 and 0.7 as suggested by Hsu et al. [16] for analogous lithology. In Table 4 are reported the estimated K values by using Eqs. 1 and 3: these values were compared and validated with available laboratory measurements performed on intact core samples drilled from representative rock outcrops and retrieved well cores. Hydraulic conductivity values were calculated based on matrix permeability values obtained from cylindrical plugs using a column gas permeameter under steady-state gas flow and at minimum of five pore fluid pressure level. Additional details can be found in Weydt et al. [9].

The results can be summarized as in the following:

- In the Rinconada Fault site, hydraulic conductivity values range between 10^{-3} m/s near the fault core zone and up to 10^{-9} m/s for the less disturbed sectors;
- There is a large difference between the K values estimated by using cubic law and HC classification, especially within the damage zone (by increasing the distance with fault, the two models provide analogous result); HC classification generally underestimates hydraulic properties in highly fractured rock masses, so results are not in agreement with other consideration for Rinconada test site.
- In Granodos Quarry test site, estimated K values are on average lower than those observed in Rinconada Fault, mirroring a massive aspect of the rock mass. Differences between K values estimated with the two models are negligible. Lab K values appears to agree better with the results of the Cubic Law results, HC results remains however in a very near range.
- In both the sites Lab K values are comparable with those estimated for massive rock mass, confirming the limitation of lab measurements, especially with highly fractured rock masses.

In Fig. 12 further insights about reliability of the proposed approach are provided, comparing the results obtained from on site and lab measurements and empirical estimations and including evidence from geophysical surveys too. For the two studied sites, rock masses were classified using GSI system [39] and as a function of the distance from the fault zone (for Rinconada Fault) or the dike (for Granados Quarry). At Rinconada Fault site, rock mass exhibit characteristics (Fig. 12a) from blocky or massive to disintegrated as a function of

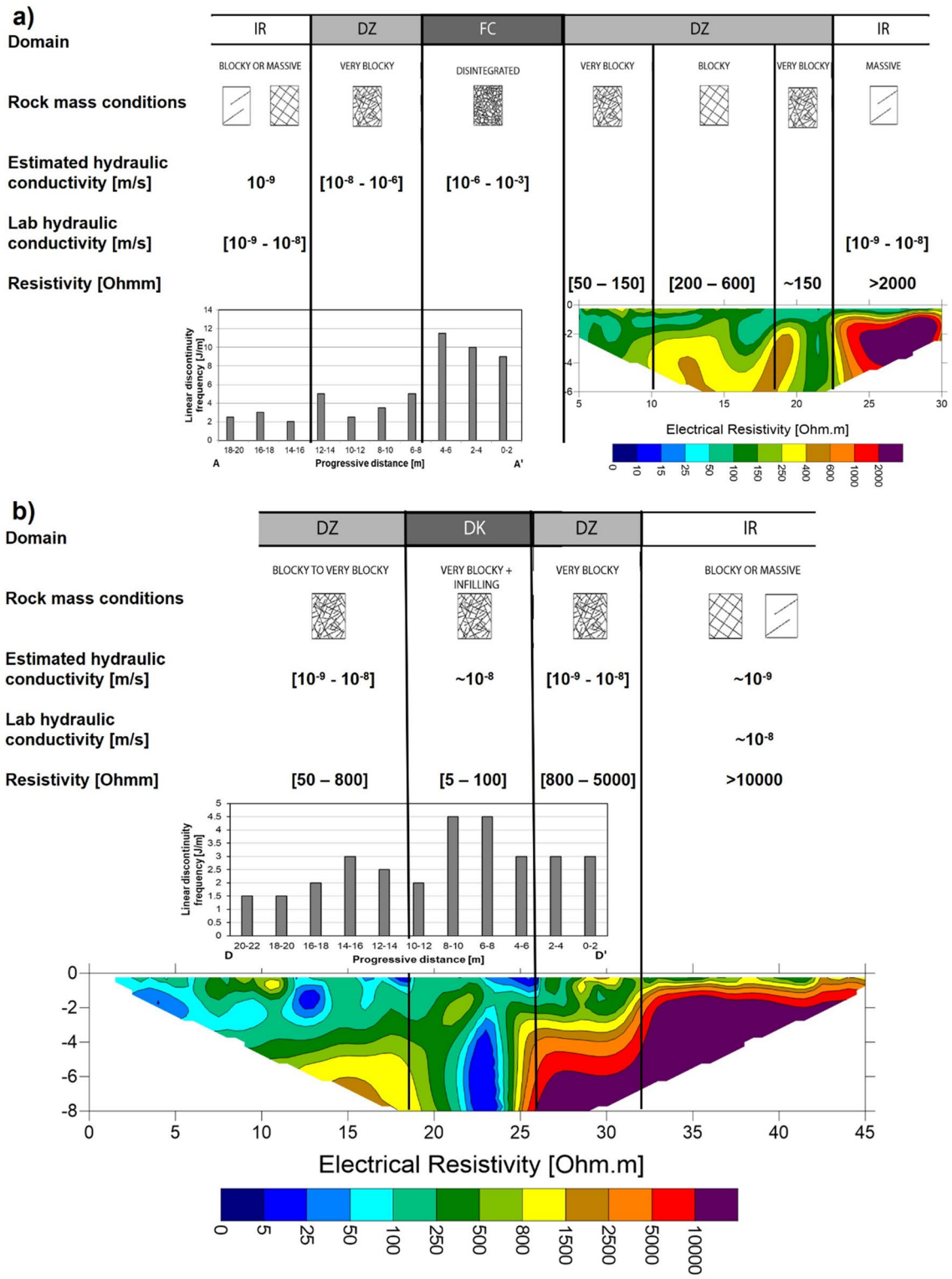


Fig. 12 Domain discretization and parameters comparison for, **a** the Rinconada Fault and **b** the Granados quarry sites

the distance from the fault. Consequently, a wide range of possible hydraulic conductivity values is expected: both cubic law model and HC classification were able to reproduce this behaviour, which is also mirrored by electrical properties variations. For Granados marble quarry site (Fig. 12b) the rock mass was discretized in

two lithological units. Nevertheless, ERT results along the survey area suggest also the presence within the andesitic unit of an intrusion dyke showing particularly low resistivity values (i.e., < 50 Ohm m). This low resistivity value suggests the presence of alterations even in the form of clay minerals. Therefore, the inner portion of the dyke may show a localized hydraulic conductivity much lower than the one within the fractured andesite (i.e., conduit-barrier model).

In the estimation of hydraulic conductivity, geomechanical and geophysical surveys cannot be considered as standalone methodologies. Indeed, the level of fracturing information provided by geomechanical characterization can lead to a misinterpretation of hydraulic conductivity, especially in the buried portion of the outcrops. For example, highly fractured outcrops could exhibit very low hydraulic conductivity at depth due to the infilling of discontinuities, which might be flushed out near the surface. Similarly, high resistivity values in ERT surveys can be mistakenly interpreted as highly fractured sectors or massive lithologies. Lower resistivity values can indicate either the presence of abundant clay materials or the presence of water circulation. The combined use of the two methodology is therefore important for confirming the evidence of one of them with respect to the other. These aspects are even clearer: at the Rinconada Fault site, the fault core exhibit moderate to low resistivity values as a consequence of extensive fluid circulation. On the other hand, for the Granados Quarry site, very blocky sectors have very low resistivity values, indicating the presence of the andesitic dike, which typically has a bulk electrical resistivity ranging from 1 to 100 Ohm m. Therefore, similar resistivity values are attributed to very different fracture settings. The discrimination of the two conditions can be solely performed by comparisons with geomechanical surveys in the same units. It is therefore not possible to establish a priori specific resistivity ranges to which attribute the different formations, but this should be a site dependent approach as a function also of the geomechanical and lithological information.

From this perspective, it is clear that the combination of the two methodologies increases the level of understanding, reduces the potential misinterpretations and provides reliable (preliminary) hydraulic conductivity values. Regarding this last point, even though we are aware that the provided hydraulic conductivity ranges, based on quantitative analyses, may not be entirely comprehensive, and further specific investigations are required, in such environmental conditions, they serve as an acceptable starting point.

7 Discussion

Heterogeneous rock masses, both due to the primary lithological differences and to the structural disposition and characteristics of the discontinuities, can experience a wide variation in hydraulic conductivity near the surface and consequently at depth. Many assessments based on laboratory analysis, which are also complex but can be carried out using different approaches and methodologies, can be found in the bibliography. The main problem, however, is the representativeness and significance of the analysed samples. This study aims at proposing a methodology that can give a first estimate of the hydraulic conductivity of the rock masses and to guide the choice of samples to be analyzed in the laboratory and in giving them the right weight in relation to the overall context. This methodology involves a detailed geomechanical characterization of the heterogeneous rock masses or fault zones exposed at the surface and ERT surveys for interpreting the buried portions at shallow depths. Although it is not possible to generalize about the depth of investigation, 10 m might be a realistic value, depending on factors such as inaccessible areas, limited space and overall geological features. Moreover, the combined methodologies are cost-effective and time-efficient, and they have provided reliable preliminary values of hydraulic conductivity. This preliminary hydrogeological characterization can be helpful for planning future analysis campaigns, both in terms of methods to be employed and locations where the tests will be performed. Regarding the two test sites, the analyses highlighted how lithological differences can be substantial and how jointing and hydraulic conductivity can change in a short distance.

For the Rinconada Fault test site, the following evidence can be found:

- There is a clear decrease in the discontinuity frequency moving away from the fault core zone, passing from more than 20 j/m near the fault to less than 5 toward the less disturbed rock sectors;
- This decrease in the discontinuity frequency is not linear, but data shows a bimodal trend: in fact, the very first 5 m from the fault are characterized by more than 10 j/m, than there is a less fractured band (about 5 j/m) 6–8 m long followed by a second more fractured band, that leave the space again to a less disturbed rock mass;
- The overall jointing trend is also highlighted in the ERT sections, showing low resistivity values (150 Ohm m) in the first 5 m from the fault, than there is an increase in resistivity (200 to 600 Ohm m),

reflecting the less fractured band 6–8 m long, followed by a second more fractured band with similar resistivity values than the first; he Rinconada Fault site is an example of how a discrete structure can be decisive in governing the geothermal fluids path: in fact, it is characterized by a 30–40 m damaged belt in which the hydraulic conductivity is definitely higher (by an order of magnitude or more) than the rest of the rock mass, even if a certain lateral variability is observed.

For the Granados Quarry test site, the following evidence can be found:

- The subvertical andesitic dyke shows a more brittle behaviour with respect to the surrounding marble with the discontinuity frequency that increase within the dyke;
- Hydraulic conductivity, if estimated only accounting for linear discontinuity frequency, would give higher values in the dyke by at least one order of magnitude;
- The resistivity values inside the dyke strongly decrease as a result of the increased water content in the infilling (probably due to the presence of alteration) mainly composed by clay.
- If the infilling is considered, the hydraulic conductivity in the weathered andesitic dyke could reach lower values than in the surrounding rock masses, thus acting as a barrier to fluid flows; this is a situation commonly encountered where clay is the infilling.

As a matter of fact, a great contribution to the overall value of the hydraulic conductivity is given by the joint opening and infilling, which are indeed very difficult to determine with precision close to the surface and which are moreover subjected to meaningful variations with depth. In Fig. 13 a conceptual resume of the findings of the study is reported. Information derived from different survey methodologies must be correctly interpreted. The results confirm a correlation between electrical resistivity and hydraulic conductivity as a function of the clayey material content, with an inverse correlation observed when the clayey content is high and a direct correlation when the fractures are open, and the infilling is negligible. The overall behaviour of the rock mass depends on the spatial relationship between different part of the faults, ranging from some decimetres to decades of metres. In the general aims of the GeMex project some studies (e.g. [42]) already focused on the dependency of fracture permeability, constrained by fracture lengths and apertures, with stress field conditions through numerical simulations populated with mechanical data and discrete fracture networks generated from Las Minas analogue outcrops.

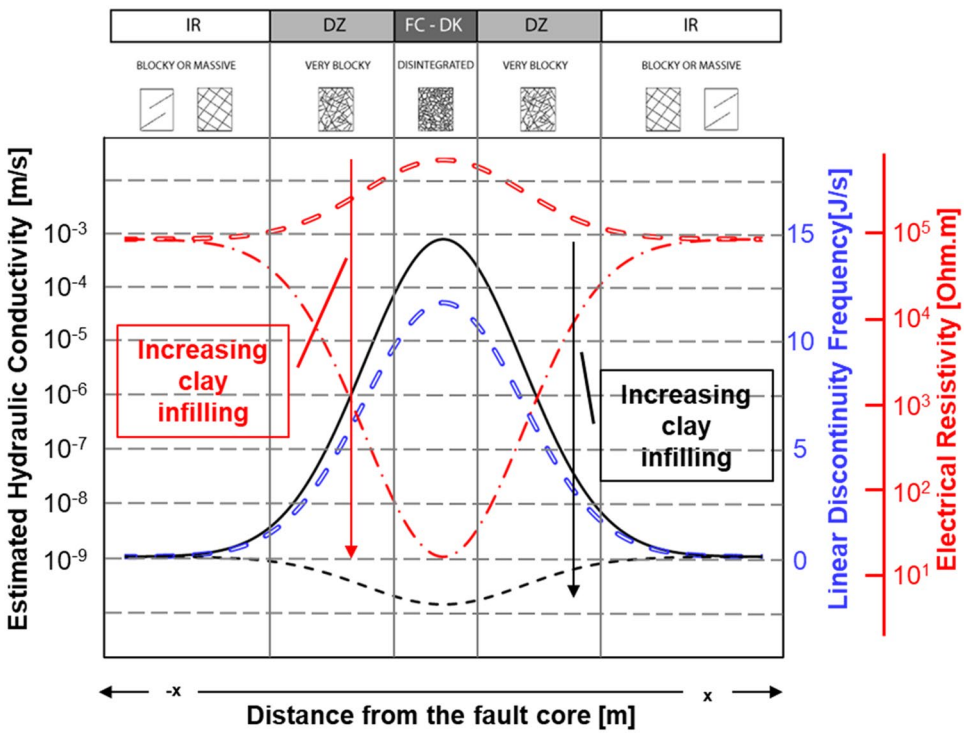


Fig. 13 Conceptual model about the variation of hydraulic conductivity based on geomechanical and geophysical field observations

8 Conclusion

Integrating the results of the two test sites, it is possible to stress some general consideration and to give some details concerning the hydraulic conductivity distribution and the general applicability of the adopted methodologies:

- Hydraulic conductivity within limestone ranges between 10^{-4} and 10^{-6} m/s or even lower, depending on the discontinuity frequency;
- Andesite shows a more brittle behaviour than the carbonatic rocks and consequently higher hydraulic conductivity values, if only the linear discontinuity frequency is used as an estimator, are expected (10^{-3} m/s); however, if the presence of clay minerals is taken in to account, the hydraulic conductivity values may substantially decrease.
- The fault core zone and the immediately adjacent sectors can reach hydraulic conductivity values up to 10^{-2} m/s.

This study testifies that field surveys are indispensable to understand technical properties of rock masses. In fact, traditional and no-contact methodologies can be integrated with each other for a better definition of the mechanical and hydrogeological properties. Moreover, it is possible to achieve information about the volume of rock perturbed by the fault-related fracturation especially if above-surface observation is coupled with near surface geophysical techniques. In fact, strong emphasis must be given to the very good agreement between physical and geophysical results: the analysis of the ERT data, even if qualitative, supports the assumptions arising from the direct observations and can be a profitable tool to be used when field observations are impossible for any reason whatsoever.

In conclusion, it is worth noting that hydraulic conductivity and/or permeability in fractured or heterogeneous rock masses is one of the most difficult parameters to infer in the absence of direct measures. The variables that may intervene are many and they may also act in opposing modes depending on the geological context. In addition, when circuits are deep, the tensional state also comes into play, which in turn affects both the opening and number of fractures. The experience that this study teaches us is that all the tools and methodologies at one's disposal must be used, and that only the integration of multiple techniques can allow to approach a reasonable and realistic result. Particularly geomechanical surveys were very important to provide a first order hydraulic conductivity estimation while geophysical surveys allowed to extend this information (and confirm it or observe changes) in the underground.

Acknowledgements The authors want to acknowledge and thank Domenico Liotta and Walter Wheeler for logistic and geological support.

Author contributions All authors contributed to the study conception and design. Material preparation, data collection and analysis were performed by in cooperation between all the authors. The first draft of the manuscript was written by GM and all authors commented on previous versions of the manuscript. All authors read and approved the final manuscript.

Funding This research was funded by European Union's EU Horizon 2020: Cooperation in Geothermal energy research Europe-Mexico for development of Enhanced Geothermal Systems and Superhot Geothermal Systems, GE-Mex [Grant Number 727550]. This project has received funding from the European Union's Horizon 2020 research and innovation programme under the grant agreement No. 727550.

Availability of data and material Data will be made available upon reasonable request to the corresponding author.

Code availability The authors don't develop any codes but they use commercial software, cited in the manuscript, for their analyses.

Declarations

Conflict of interest The authors have no competing interests to declare that are relevant to the content of this article.

Open Access This article is licensed under a Creative Commons Attribution 4.0 International License, which permits use, sharing, adaptation, distribution and reproduction in any medium or format, as long as you give appropriate credit to the original author(s) and the source, provide a link to the Creative Commons licence, and indicate if changes were made. The images or other third party material in this article are included in the article's Creative Commons licence, unless indicated otherwise in a credit line to the material. If material is not included in the article's Creative Commons licence and your intended use is not permitted by statutory regulation or exceeds the permitted use, you will need to obtain permission directly from the copyright holder. To view a copy of this licence, visit http://creativecommons.org/licenses/by/4.0/.

References

1. Chicco J, Vacha D, Mandrone G (2019) Thermo-physical and geomechanical characterization of faulted carbonate rock masses (Valdieri, Italy). Remote Sens 11:179. https://doi.org/10.3390/rs11020179
2. Rybach L, Muffler LJP (1981) Geothermal systems: principles and case histories. Wiley-Interscience, Chichester, England
3. Turnadge C, Mallants D, Peeters L (2018) Overview of aquitard and geological fault simulation approaches in regional scale assessments of coal seam gas extraction impacts. Commonwealth scientific and industrial research organisation (CSIRO), Canberra
4. Underschultz J, Esterle J, Strand J, Hayes S (2018) Conceptual representation of fluid flow conditions associated with faults in

sedimentary basins. University of Queensland Centre for Coal Seam Gas, Queensland
5. Bense VF, Gleeson T, Loveless SE et al (2013) Fault zone hydrogeology. Earth Sci Rev 127:171–192. https://doi.org/10.1016/j.earscirev.2013.09.008
6. Rawling GC, Goodwin LB, Wilson JL (2001) Internal architecture, permeability structure, and hydrologic significance of contrasting fault-zone types. Geology 29(1):43–46. https://doi.org/10.1130/0091-7613(2001)029%3c0043:IAPSAH%3e2.0.CO;2
7. Piscopo V, Baiocchi A, Lotti F et al (2018) Estimation of rock mass permeability using variation in hydraulic conductivity with depth: experiences in hard rocks of western Turkey. Bull Eng Geol Environ 77:1663–1671. https://doi.org/10.1007/s10064-017-1058-8
8. Zhu J, Yeh T-CJ (2006) Analysis of hydraulic tomography using temporal moments of drawdown recovery data. Water Resour Res 42:W02403. https://doi.org/10.1029/2005WR004309
9. Weydt LM, Ramírez-Guzmán ÁA, Pola A et al (2021) Petrophysical and mechanical rock property database of the Los Humeros and Acoculco geothermal fields (Mexico). Earth Syst Sci Data 13:571–598. https://doi.org/10.5194/essd-13-571-2021
10. Snow DT (1968) Rock fracture spacings, openings, and porosities. J Soil Mech Found Div 94:73–91. https://doi.org/10.1061/JSFEAQ.0001097
11. Louis C (1972) Rock hydraulics. Rock mechanics. Springer Vienna, Vienna, pp 299–387
12. Burgess A (1977) Groundwater movements around a repository. Stockholm (Sweden)
13. Carlssn L, Winberg A, Rosander B (1983) Investigations of hydraulic properties in crystalline rock. MRS Proc 26:255. https://doi.org/10.1557/PROC-26-255
14. Black JH (1987) Flow and flow mechanisms in crystalline rock. Geol Soc 34:185–200. https://doi.org/10.1144/GSL.SP.1987.034.01.13
15. Wei ZQ, Egger P, Descoeudres F (1995) Permeability predictions for jointed rock masses. Int J Rock Mech Min Sci Geomech Abstr 32:251–261. https://doi.org/10.1016/0148-9062(94)00034-Z
16. Hsu S-M, Lo H-C, Chi S-Y, Ku C-Y (2011) Rock mass hydraulic conductivity estimated by two empirical models. In: Developments in hydraulic conductivity research. InTech. https://doi.org/10.5772/15669
17. Gates WCB (1997) The hydro-potential (HP) value: a rock classification technique for evaluation of the ground-water potential in fractured bedrock. Environ Eng Geosci III:251–267. https://doi.org/10.2113/gseegeosci.III.2.251
18. Shahbazi A, Saeidi A, Chesnaux R (2020) A review of existing methods used to evaluate the hydraulic conductivity of a fractured rock mass. Eng Geol 265:105438. https://doi.org/10.1016/J.ENGGEO.2019.105438
19. Roe P (2017) Is discontinuous reconstruction really a good idea? J Sci Comput 73:1094–1114. https://doi.org/10.1007/s10915-017-0555-z
20. Snow DT (1969) Anisotropie permeability of fractured media. Water Resour Res 5:1273–1289. https://doi.org/10.1029/WR005i006p01273
21. Demanet D, Renardy F, Vanneste K et al (2001) The use of geophysical prospecting for imaging active faults in the Roer Graben, Belgium. Geophysics 66:78–89. https://doi.org/10.1190/1.1444925
22. Vanneste K, Verbeeck K, Petermans T (2008) Pseudo-3D imaging of a low-slip-rate, active normal fault using shallow geophysical methods: the geleen fault in the Belgian Maas river valley. Geophysics 73:B1–B9. https://doi.org/10.1190/1.2816428
23. Chaudhuri A, Sekhar M, Descloitres M et al (2013) Constraining complex aquifer geometry with geophysics (2-D ERT and MRS measurements) for stochastic modelling of groundwater flow. J Appl Geophy 98:288–297. https://doi.org/10.1016/J.JAPPGEO.2013.09.005
24. Belle P, Lachassagne P, Mathieu F et al (2019) Characterization and location of the laminated layer within hard rock weathering profiles from electrical resistivity tomography: implications for water well siting. Geol Soc 479:187–205. https://doi.org/10.1144/SP479.7
25. Withman D, Yeboah-Forson A (2015) Electrical resisitivity and porosity structure of the upper Biscayne Aquifer in Miami-Dade County, Florida. J Hydrol 531:781–791. https://doi.org/10.1016/j.jhydrol.2015.10.049
26. Descloitres M, Ruiz L, Sekhar M et al (2008) Characterization of seasonal local recharge using electrical resistivity tomography and magnetic resonance sounding. Hydrol Process 22:384–394. https://doi.org/10.1002/hyp.6608
27. Mézquita González JA, Comte JC, Legchenko A et al (2021) Quantification of groundwater storage heterogeneity in weathered/fractured basement rock aquifers using electrical resistivity tomography: sensitivity and uncertainty associated with petrophysical modelling. J Hydrol (Amst) 593:125637. https://doi.org/10.1016/J.JHYDROL.2020.125637
28. Singh U, Sharma PK (2022) Seasonal groundwater monitoring using surface NMR and 2D/3D ERT. Environ Earth Sci 81:198. https://doi.org/10.1007/s12665-022-10325-9
29. Leopold M, Völkel J, Huber J, Dethier D (2013) Subsurface architecture of the boulder creek critical zone observatory from electrical resistivity tomography. Earth Surf Process Landf n/a-n/a. https://doi.org/10.1002/esp.3420
30. Flinchum BA, Holbrook WS, Grana D et al (2018) Estimating the water holding capacity of the critical zone using near-surface geophysics. Hydrol Process 32:3308–3326. https://doi.org/10.1002/hyp.13260
31. ISRM (2015) The ISRM suggested methods for rock characterization, testing and monitoring: 2007–2014. Springer International Publishing, Cham
32. Olvera-García E, Bianco C, Víctor Hugo G-M et al (2020) Geology of Las Minas: an example of an exhumed geothermal system (Eastern Trans-Mexican Volcanic Belt). J Maps 16:918–926. https://doi.org/10.1080/17445647.2020.1842815
33. Jolie E, Gutierrez-Negrin LC, Liotta D, Arango-Galvan C, Pall Hersir G et al (2020) The GEMex project: developing Los Humeros (Mexico) as a Superhot Geothermal Site. Proceedings World geothermal Congress 2020+1, Reykjavik, Iceland, April-October 2021
34. Cedillo-Rodríguez F (1997) Geologia del subsuelo del campo geotermico de Los Humeros, Pue. Internal Report HU/RE/03/97. Comision Federal de Electricidad, Gerencia deProyectos Geotermoelectricos, Residencia Los Humeros, Puebla, p 30
35. Arzate J, Corbo-Camargo F, Carrasco-Núñez G et al (2018) The Los Humeros (Mexico) geothermal field model deduced from new geophysical and geological data. Geothermics 71:200–211. https://doi.org/10.1016/J.GEOTHERMICS.2017.09.009
36. Norini G, Carrasco-Núñez G, Corbo-Camargo F et al (2019) The structural architecture of the Los Humeros volcanic complex and geothermal field. J Volcanol Geoth Res 381:312–329. https://doi.org/10.1016/J.JVOLGEORES.2019.06.010
37. Liotta D, Bastesen E, Bianco C et al (2021) Analogue geothermal systems in Mexico: insights into the deep part of Los Humeros geothermal field from the Las Minas mining area (Eastern Mexico). Proceeding World Geothermal Congress, Reykjavik, Iceland October 2021
38. Castro Mora J, Ortiz-Hernández LE, Escamilla-Casas JC et al (2016) Metalogénesis de la mineralización tipo IOCG relacionada al SKARN del distrito minero las minas, Estado de Veracruz. Tópicos de Investigación en Ciencias de la Tierra y Materiales. 3:128–143. https://doi.org/10.29057/aactm.v3i3.9617

39. Hoek E, Brown ET (1997) Practical estimates of rock mass strength. Int J Rock Mech Min Sci 34:1165–1186. https://doi.org/10.1016/S1365-1609(97)80069-X
40. Dershowitz WS, Herda HH (1992) Interpretation of fracture spacing and intensity. In: Tillerson JR, Wawersik WR (eds) Rock Mechanics. Balkema AA, Rotterdam, pp 757–766
41. Hoek E, Bray JD (1981) Rock slope engineering, 3rd edn. The institution of mining and metallurgy, London, pp 341–351
42. Lepillier B, Daniilidis A, Doonechaly Gholizadeh N et al (2019) A fracture flow permeability and stress dependency simulation applied to multi-reservoirs, multi-production scenarios analysis. Geotherm Energy 7:24. https://doi.org/10.1186/s40517-019-0141-8

Publisher's Note Springer Nature remains neutral with regard to jurisdictional claims in published maps and institutional affiliations.